Cross-Validation of Computational and Experimental Distributed Surface Pressures on the Space Launch System

Morgan A. Walker*, Michael W. Lee*, and Lee J. Mears*

NASA Langley Research Center, Hampton, VA 23681

This paper presents a new workflow for comparing experimental pressure-sensitive paint (PSP) data to computational fluid dynamic (CFD) simulations by way of mapping data from corresponding surface grids utilizing interpolation methods. In addition to generating quantitative and qualitative point-to-point comparisons between PSP and CFD data, this workflow extracts sectional loading data from both surface grids and generates lineload comparison charts for corresponding PSP and CFD runs. Experimental PSP data presented in this paper were from a 2016 test of the NASA Space Launch System in the 11- by 11-Foot Transonic Wind Tunnel section of the NASA Ames Unitary Plan Wind Tunnel complex. CFD simulation data for comparison purposes were generated using the FUN3D code. Overall, interpolation onto PSP surface grids versus CFD surface grids yields comparable surface pressure fields. However, lineload comparisons are easier to make on the CFD grid-mapped data due to the surface grid topology and the current capabilities of the lineload analysis tools at the NASA Langley Research Center. This workflow is written using contemporary software (Python, Tecplot, PyTecplot), is compatible with existing tools at NASA Langley, and is developed to be adaptable depending on the situation.

Nomenclature

ARC	=	Ames Research Center
ATT	=	Aerodynamics Task Team
CFD	=	Computational Fluid Dynamics
CGT	=	Chimera Grid Tools
C^0	=	integration scheme, derived from midpoint rule
C^1	=	integration scheme, derived from trapezoid rule
C_p	=	surface pressure coefficient
CA_{LL}	=	axial force coefficient, lineload
CN_{LL}	=	normal force coefficient, lineload
CY_{LL}	=	side force coefficient, lineload
$LaRC$	=	Langley Research Center
$\vec{ll}_p(x)$	=	lineload of pressure component in x-direction
$\vec{lm}_p(x)$	=	line moment of pressure component in x-direction
M_∞	=	freestream Mach number
$\hat{n}$	=	elementwise unit normal vector on surface S
PSP	=	Pressure-sensitive Paint
$\vec{r}$	=	moment arm vector
Re_D	=	Reynolds number based on core diameter
Re_u	=	unit Reynolds number per foot
S	=	lineload integrating surface
SLS	=	Space Launch System
SRB	=	Solid Rocket Booster
$uPSP$	=	Unsteady Pressure-sensitive Paint
$UPWT$	=	Unitary Plan Wind Tunnel
α_V	=	angle of attack in the vertical-plane axis system, deg
β_V	=	angle of sideslip in the vertical-plane axis system, deg
ΔC_p	=	surface pressure coefficient difference

*Research Aerospace Engineer, Configuration Aerodynamics Branch, NASA Langley Research Center, AIAA Member.

I. Introduction

The Space Launch System (SLS) is a super-heavy-lift launch vehicle currently under development by NASA [1]. The SLS Program is intended to comprise a series of launch vehicles that will serve as the platform of choice for modern human space exploration. These vehicles share a common liquid fuel core stage, and each have two solid rocket boosters (SRB) attached. The upper stage can be swapped interchangeably depending on mission requirements. An artist rendering of the various configurations of the SLS is presented in Fig. 1.

Throughout the course of the SLS program, the SLS Aerodynamics Task Team (ATT) has been tasked with the development of many different aerodynamic databases. These databases include, but are not limited to, information such as aerodynamic loads, lineloads, core base pressures, SRB hinge moments, and buffet forcing functions, and are intended to help qualify the induced environments experienced by the SLS throughout the entire launch and reentry process. To accomplish this goal, the ATT relies on a combination of data acquired through numerous wind tunnel tests at different facilities and conditions in conjunction with results from computational fluid dynamics (CFD) simulations using a variety of different codes.

When creating a database, the transonic flight regime has historically been difficult to model due to the potentially changing flow physics as the SLS transitions from subsonic to supersonic speeds during the ascent phase. In particular, the surface pressures are difficult to quantify in this region. As such, databases typically rely on CFD simulations to describe this environment. Surface pressure taps can be used to collect experimental data in this region, but an unfeasible amount of taps would be needed to obtain the type of high-fidelity surface pressure data needed to calculate information such as lineloads. This issue is especially difficult around the SRB attach points, where the flow physics can be difficult to model at transonic conditions.
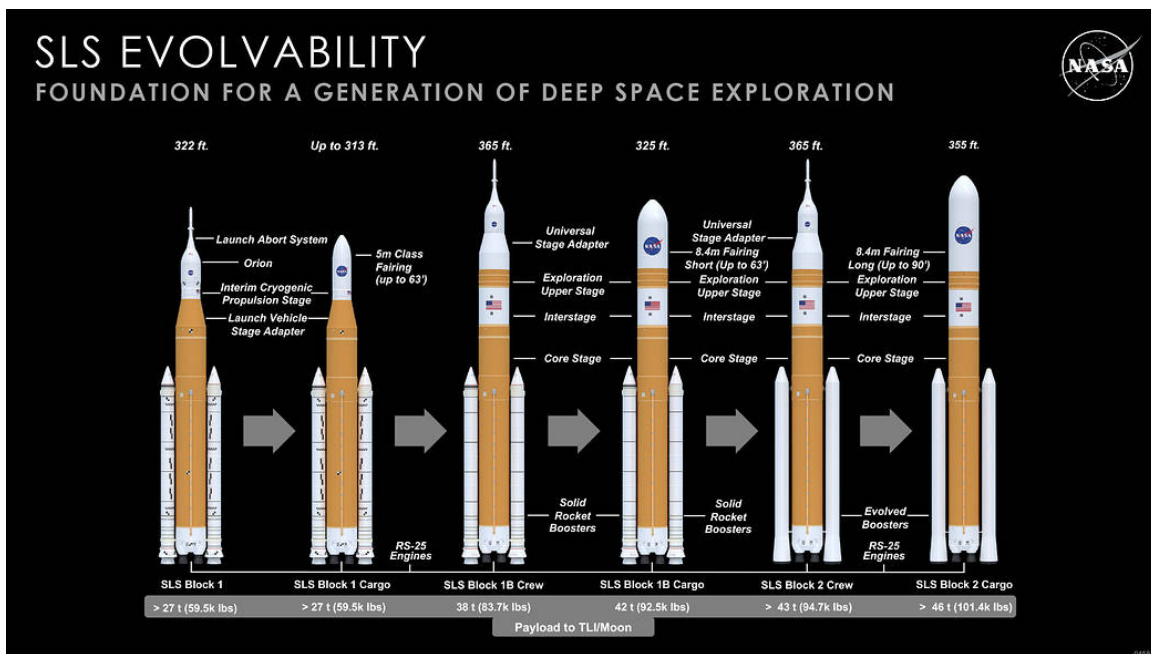

Fig. 1   Artist rendering of the evolving SLS configurations [1].

In response to the desire to validate CFD surface pressure data against an experimental method, the usage of pressure-sensitive paint (PSP) has been introduced into several different SLS wind tunnel tests over the past five years. Efforts have been made in the past [2] to compare PSP and CFD data. These comparisons demonstrated decent agreement between the methods, with some notable differences occuring around protuberances and areas of high curvature. PSP data have successfully been collected at the NASA Ames Research Center (ARC) Unitary Plan Wind Tunnel (UPWT) and the NASA Langley Research Center (LaRC) UPWT, and are planned for use in future tests to continue to develop the method. Another application of PSP is for use in unsteady flows (uPSP). NASA has also used uPSP to successfully acquire data in the past, although data processing methods are still in development [3].

II. Methodology

Independent workflows have been developed previously to compare PSP and CFD data [2] using a Tecplot-based approach, as well as to compute lineloads using the *TRILOAD* routine in the Chimera Grid Tools (CGT) package [4]. This section introduces the new methodology developed that explores different interpolation methods to compare PSP and CFD data and streamlines the process of computing lineloads from the resulting surface grids. Note that the PSP and CFD data used in development of the new workflow were the same data from the ARC UPWT 11- by 11-Foot Transonic Wind Tunnel (11-Ft TWT) test utilized in [2], [4]. This allows for more direct comparisons to be made between the methods as well as providing another set of data for validation. A layout of the 11-Ft TWT facility is shown in Fig. 2. The 1.3%-scale model of the SLS Block 1B Crew configuration with PSP applied in the 11-Ft TWT test section is shown in Fig. 3. Further details on this test and the 11-Ft TWT are outlined in [5], [6], [7], [8].
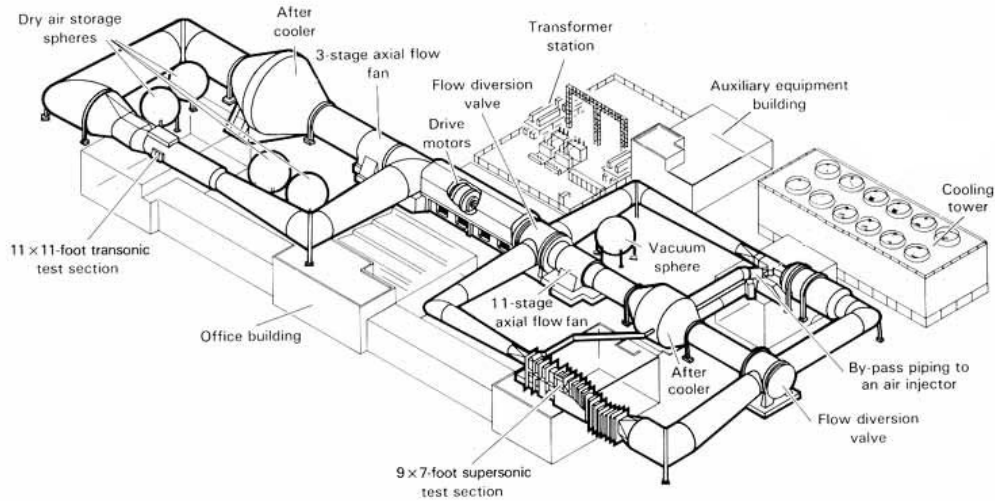

Fig. 2   NASA ARC UPWT site layout.

Fig. 3   SLS Block 1B Crew model with PSP applied to model in the NASA ARC 11-Ft TWT.

A. Interpolation

PSP and CFD data were both mapped onto their corresponding surface grids. While both grids model the same SLS wind tunnel configuration, their compositions are different. These differences are represented visually in Fig. 4. The PSP surface grid is composed of many different structured zones of rectangles, while the CFD surface grid is composed of a few unstructured zones of triangles. Each set of surface grids is generated by different teams within NASA, with the structure determined to best suit the needs of that team. As such, the PSP and CFD surface grids cannot be compared directly, but interpolation methods can be used to either map the CFD data onto the PSP surface grid, or to map the PSP data onto the CFD surface grid.
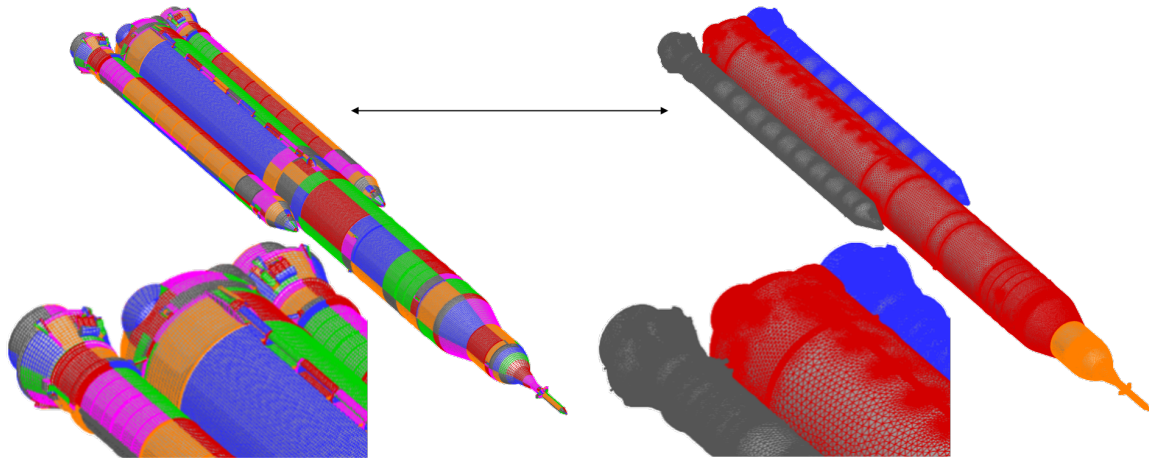

Fig. 4   Visual comparison of PSP surface grid (left) and CFD surface grid (right).

Due to the experimental nature of the PSP data, not all regions of the model have PSP data associated with them for a particular wind tunnel run. This is because there are regions of the wind tunnel model such as between the SRBs and core and underneath liquid oxygen feed lines that are shadowed from the view of the PSP cameras. As such, the PSP surface grid has several shadowed zones on it where CFD data cannot be mapped. Conversely, a lack of PSP data at these locations means that there are a few places where PSP pressure distributions are interpolated from the surrounding unblanked regions when mapping onto the CFD surface grid. These shadowed regions are shown in Fig. 5. Note that the shadowed regions and their associated lack of data do not significantly affect comparison efforts, they are simply a byproduct of the model geometry and the PSP camera system.
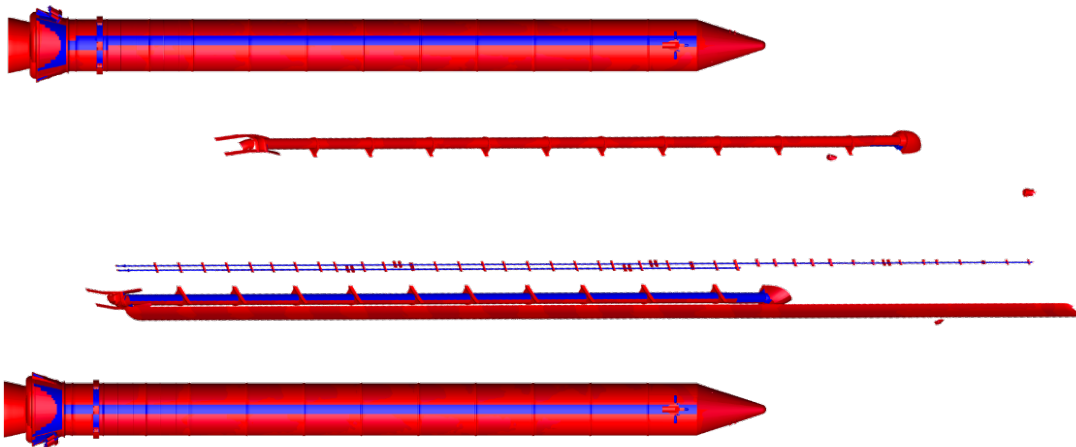

Fig. 5   Shadowed regions (in blue) without PSP data.

1. PSP-to-CFD Grid

As a first step in mapping data from the PSP surface grid to the CFD surface grid, the corresponding point pairs between wind tunnel and CFD runs must be identified. These pairs are difficult to identify visually as the CFD data are formatted in missile coordinates, while the wind tunnel data uses tunnel coordinates. A Python script has been developed to convert the CFD angles into tunnel angles, and then match point pairs together by ensuring both points were at the same Mach (M_∞), angle of attack (α_V), angle of sideslip (β_V), and unit Reynolds number (Re_u) conditions.

After the point pairs are identified, a PyTecplot script is called to rezone the PSP data onto the CFD surface grid. While both the CFD and wind tunnel geometries are identical, they are not in the same scale. In this case, the PSP data were acquired at the 1.3% wind tunnel model scale, and had to be rescaled and translated into the full-scale coordinates used in the CFD surface grid. After the PSP data are rescaled, the inverse distance function is called in Tecplot to interpolate the PSP zonal data onto the CFD surface grid. The inverse distance method was selected over the linear interpolation option due to speed of processing while maintaining a similar accuracy [9]. Shadowed zones within the PSP data are not included in the interpolation process.

Following the interpolation process, the M_∞, α_V, β_V, and Re_u values are saved within the auxiliary data in Tecplot to allow for quick confirmation that both the wind tunnel and CFD runs are at the same condition. Following this, the PyTecplot script saves the completed grid as a *<filename>.plt* file and repeats the process of rescaling and interpolating the remaining point pairs in a batch-processing style, saving on user time and effort. The end result is the creation of a series of CFD surface grids with corresponding wind tunnel PSP data interpolated onto them. This allows for point-to-point comparisons to be made between the original CFD data and PSP-interpolated data at the same condition on the same CFD surface grid. This is a new development that has not been explored in previous research. An example of PSP data interpolated onto a CFD surface grid is shown in Fig. 6.
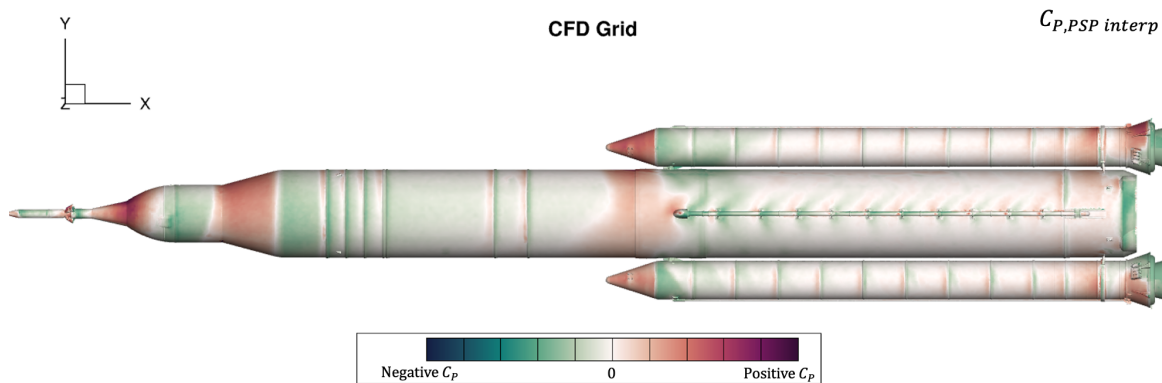

Fig. 6   PSP data interpolated onto the CFD surface grid at M_∞ = 1.3, α_V = 0°, β_V = 8°, and Re_u = 3 x 10⁶/ft.

2. CFD-to-PSP Grid

A similar scripting process has been developed in PyTecplot to map data from the CFD surface grid to the PSP surface grid. After the point pairs are identified using the aforementioned script in the previous section, a separate PyTecplot script is called to rezone the CFD data onto the PSP surface grid. In this case, the full-scale CFD data were scaled down to the 1.3% wind tunnel model scale, and the inverse distance function in Tecplot was used to interpolate the CFD zonal data onto the PSP surface grid.

The interpolation of the CFD data onto the PSP surface grid allows for similar point-to-point comparisons to be made between the original PSP data and CFD-interpolated data at the same condition on the same PSP surface grid. Having these two sets of data on the same grid allows for differences to be calculated between them, and further comparisons can be made between these differences and the differences calculated on the PSP-to-CFD grids. The CFD-interpolated pressure data at the same condition and with the same scale as Fig. 6 are presented in Fig. 7. Note that there are many similarities between the two figures, which shows that there is good agreement between both interpolated data sets at the same condition.
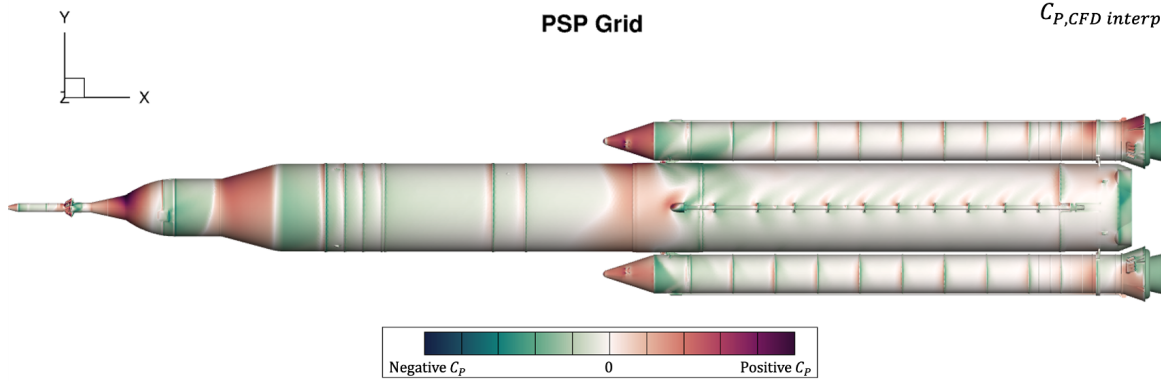
Fig. 7 CFD data interpolated onto the PSP surface grid at M_∞ = 1.3, α_V = 0°, β_V = 8°, and Re_u = 3 x 10⁶/ft.

B. Lineloads

In addition to the pointwise contours discussed above, the coexistence of PSP and CFD on a common grid enables comparison of results via lineloads. Lineloads, or sectional loads, are created by integrating the surface stress tensor – in this case just the (diagonal) pressure component – in two of the three spatial dimensions:

$$\vec{ll}_p(x) \equiv \int_S C_p \hat{n} \, dy dz \qquad (1)$$

where S is the body surface defined by normals $\hat{n}$ and in this case the pressure lineload is defined along the x-axis. This resulting lineload can then be integrated along the final axis to obtain the integrated forces. Line moments can likewise be calculated:

$$\vec{lm}_p(x) \equiv \int_S \vec{r} \times (C_p \hat{n}) \, dy dz \ . \qquad (2)$$

where $\vec{r}$ is the moment vector. Several tools exist to calculate lineloads from surface data, including a subset of Chimera Grid Tools [10], [11] and a new standalone Python-based tool developed at NASA LaRC [9]. The former was used by Meeroff et al. [4] and the latter is integrated as part of the new workflow outlined here.

The CFD surface grids in this work are all triangular in nature and are thus compatible with the new Python-based tool. Like other tools, it segregates the grid into bins along the axis of interest and then integrates the values in each bin to create the lineload. The numerical integration is mathematically C^0, which is equivalent to a Riemann sum.

III. Results

Using the newly developed workflow, PSP/CFD comparisons were generated for the data acquired in the ARC 11-Ft TWT. The range of Mach numbers tested was between M_∞ = 0.8 and M_∞ = 1.3, and the configurations tested were the SLS Block 1 Crew, Block 1B Cargo, and Block 1B Crew. This paper will present results from the Block 1B Crew configuration. Baseline case results have been presented in previous work [2], so a condition where more pronounced differences were observed between CFD and PSP data will be presented. Data from only one side of the SLS will be presented, as data from the other side exhibits similar behaviors and patterns that do not merit their own separate discussion.

A. Interpolation

Figure 8 shows the ΔC_p contour between the PSP-interpolated data on the CFD surface grid and the original CFD data at M_∞ = 1.3, α_V = 0°, β_V = 8°, Re_u = 3 x 10⁶/ft, and Re_D = 1.08 x 10⁶. The ΔC_p data show the agreement between the PSP-interpolated data and the CFD data is strong. A lack of deep shades of reds and blues on this contour indicates that there are no significant differences between the C_p values calculated from the two methods and interpolated onto the same grid. Overall, the PSP-interpolated data tends to have a higher C_p than the CFD data, although the opposite is true toward the Launch Abort System/Multi-Purpose Crew Vehicle (LAS/MPCV) and forward

SRB attachment point regions. In addition, the largest differences appear to occur around locations where large ridges (e.g., SRB rings, stiffener and joint rings, LAS rings, etc.) are present in the model, where the PSP-interpolated data registers a much lower C_p than the CFD data.
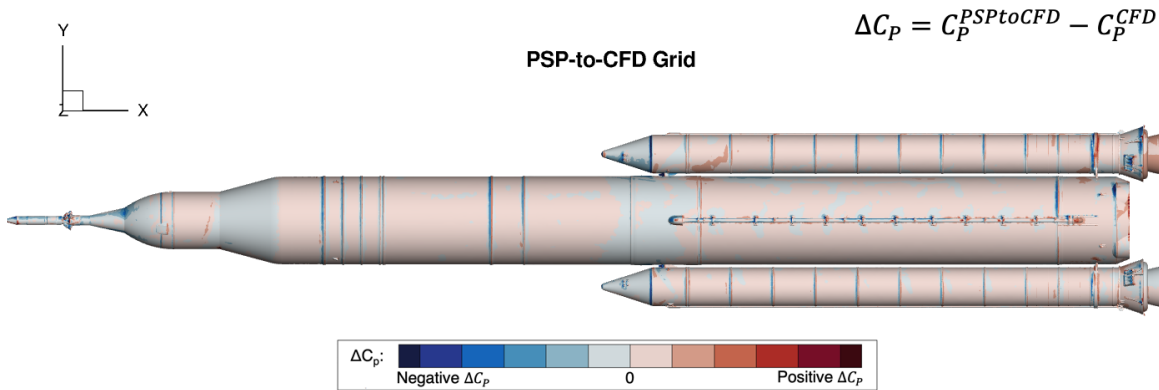

$$\Delta C_P = C_P^{PSPtoCFD} - C_P^{CFD}$$

PSP-to-CFD Grid

Fig. 8 ΔC_p **between PSP data interpolated onto the CFD surface grid and CFD data at** M_∞ **= 1.3,** α_V **= 0°,** β_V **= 8°, and** Re_u **= 3 x 10^6/ft.**

Figure 9 shows the ΔC_p contour between the original PSP data and the CFD-interpolated data on the PSP surface grid at M_∞ = 1.3, α_V = 0°, β_V = 8°, Re_u = 3 x 10^6/ft, and Re_D = 1.08 x 10^6. Once again, the agreement between the original and interpolated data sets is strong, indicating that there are no significant differences in C_p between the two methods. Unlike Fig. 8, Fig. 9 shows several shadowed regions present toward the aft SRB nozzles. These shadowed regions lead to a high ΔC_p, but this is simply because the shadowed regions are assigned a value of 9.99 in the PSP data, producing artificially high differences. Ignoring these regions, Figs. 8 and 9 show very strong agreement when compared to each other. Both figures exhibit almost identical patterns, which suggest that both interpolation methods were performed correctly. Theoretically, it shouldn't matter which data set is interpolated onto which grid, the differences should be the same.
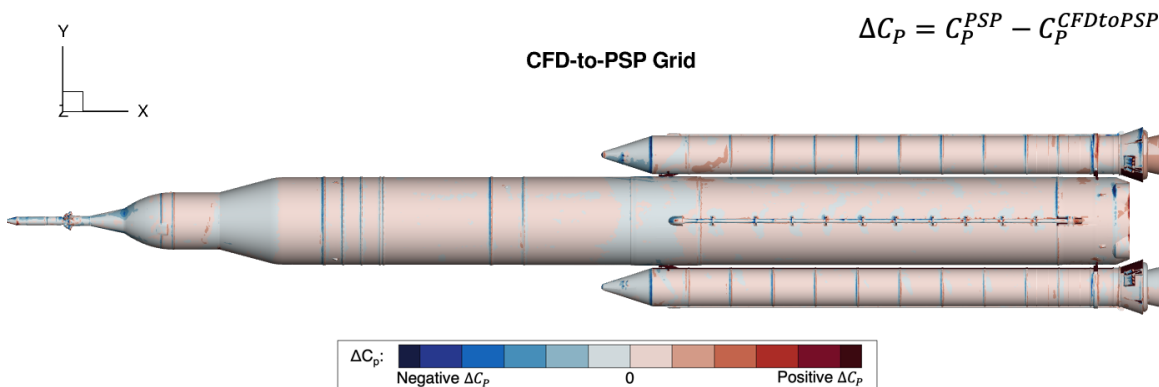

$$\Delta C_P = C_P^{PSP} - C_P^{CFDtoPSP}$$

CFD-to-PSP Grid

Fig. 9 ΔC_p **between PSP data and CFD data interpolated onto the PSP surface grid at** M_∞ **= 1.3,** α_V **= 0°,** β_V **= 8°, and** Re_u **= 3 x 10^6/ft.**

While both grids appear to exhibit almost identical behavior when comparing ΔC_p contours to each other, this is not exactly the case. Figure 10 provides a side-by-side comparison between both grids, but with a 5x-tightened scale to help magnify the differences between the grids and allow for easier point-to-point comparisons. The run condition remains M_∞ = 1.3, α_V = 0°, β_V = 8°, Re_u = 3 x 10^6/ft, and Re_D = 1.08 x 10^6. While both interpolation methods yield very similar results, there are notable differences in the ΔC_p contours. Overall, the data mapped to the CFD surface

grid are more continuous with smoother transitions between ΔC_P values, while the data mapped to the PSP surface grid are patchier in some locations and produce less straight lines. These differences are likely caused by the different grid sizes and compositions. The PSP-to-CFD grid is larger and has a higher resolution than the CFD-to-PSP grid. The most notable regions with potential differences are the forward SRB region, the aft SRB region, and the LAS/MPCV region.
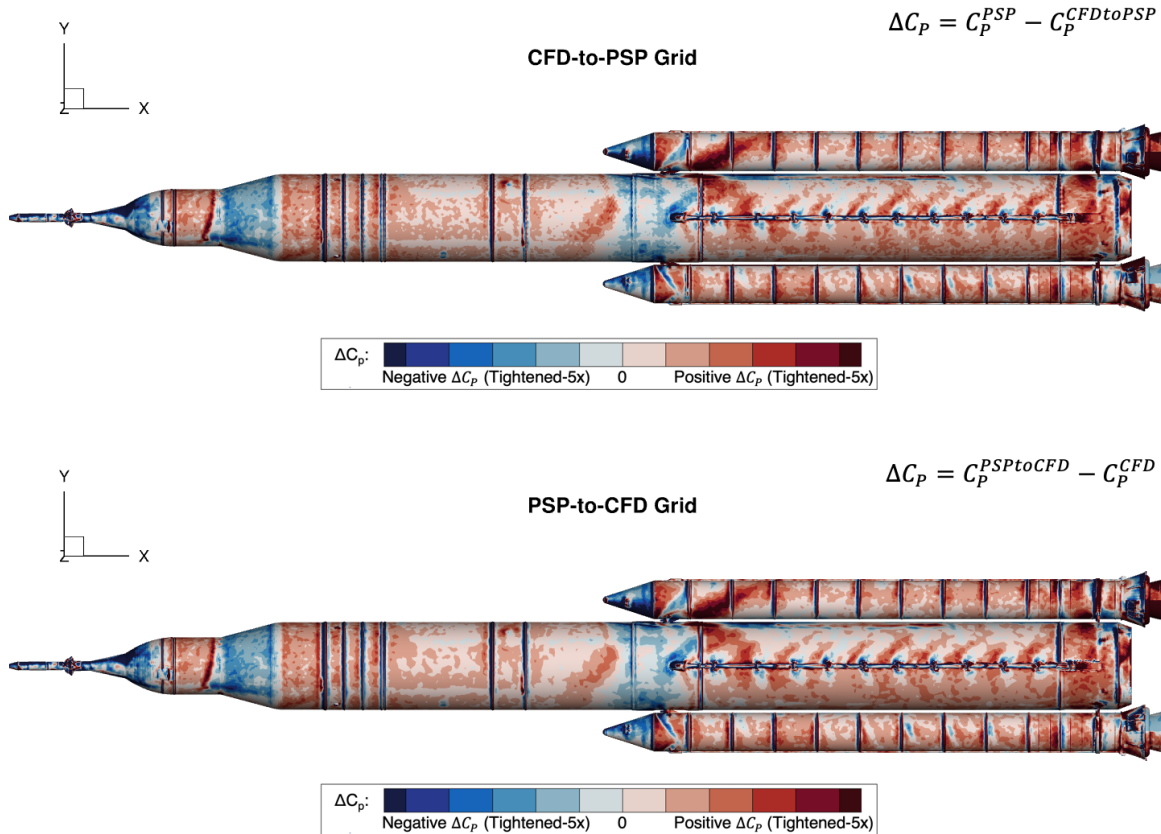

$$\Delta C_P = C_P^{PSP} - C_P^{CFDtoPSP}$$

$$\Delta C_P = C_P^{PSPtoCFD} - C_P^{CFD}$$

Fig. 10 ΔC_p **for each interpolation method (5x-tightened scale) at** M_∞ **= 1.3,** α_V **= 0°,** β_V **= 8°, and** Re_u **= 3 x** 10^6**/ft.**

1. Forward SRB Region

    Figure 11 shows a side-by-side comparison between the forward SRB region for both grids at M_∞= 1.3, α_V = 0°, β_V = 8°, Re_u = 3 x 10^6/ft, and Re_D = 1.08 x 10^6. While the overall contours follow a very similar pattern between both grids, this view demonstrates the patchier nature of the CFD-to-PSP grid data when compared to the PSP-to-CFD grid. The most notable differences as a result of the grids being different occur along the ridges of the SRBs and core. Traveling in the +X direction, PSP appears to consistently measure lower C_p values compared to CFD right before hitting the ridge, and consistently measure higher C_p values immediately after. On the PSP-to-CFD grid, the ΔC_p contours are straight and follow the same curvature as the ridges. On the CFD-to-PSP grid, however, the ΔC_p contours are wavy and not as smooth as their counterparts. It is unclear why this is the case, but one explanation is that the higher-resolution CFD surface grid was able to resolve the smoothness of the line better than the lower-resolution PSP surface grid.
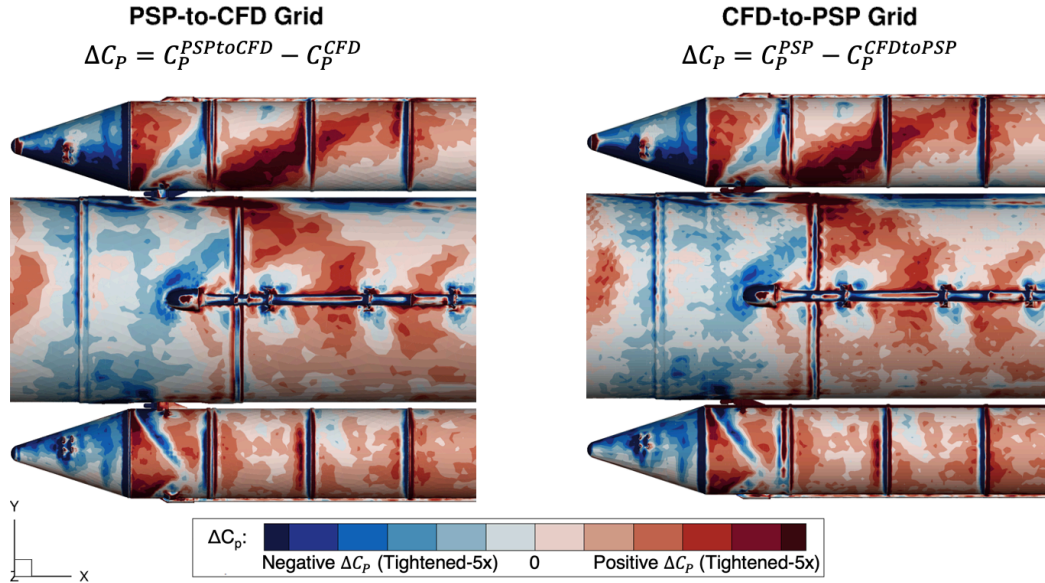
PSP-to-CFD Grid
$$\Delta C_P = C_P^{PSPtoCFD} - C_P^{CFD}$$

CFD-to-PSP Grid
$$\Delta C_P = C_P^{PSP} - C_P^{CFDtoPSP}$$

ΔC_p:
Negative ΔC_P (Tightened-5x)   0   Positive ΔC_P (Tightened-5x)

Fig. 11   Forward SRB region at M_∞ = 1.3, α_V = 0°, β_V = 8°, and Re_u = 3 x 10⁶/ft.

2. Aft SRB Region

Figure 12 shows a side-by-side comparison between the aft SRB region for both grids at M_∞ = 1.3, α_V = 0°, β_V = 8°, Re_u = 3 x 10⁶/ft, and Re_D = 1.08 x 10⁶. Once again, the PSP-to-CFD grid shows smoother and less patchiness than the CFD-to-PSP grid. It should be noted that the ΔC_p data around the core-facing sides of the SRB nozzles for both grids exhibit behavior that is inconsistent with the rest of the model. This is likely an artifact of poor PSP data quality collected around these regions during the test. Referring to Fig. 5, it shows that this region is intermittently shadowed around these locations, and this shadowing may have adversely affected the data. As such, CFD data alone should be used when analyzing the C_p contours around this area, as PSP is limited here.
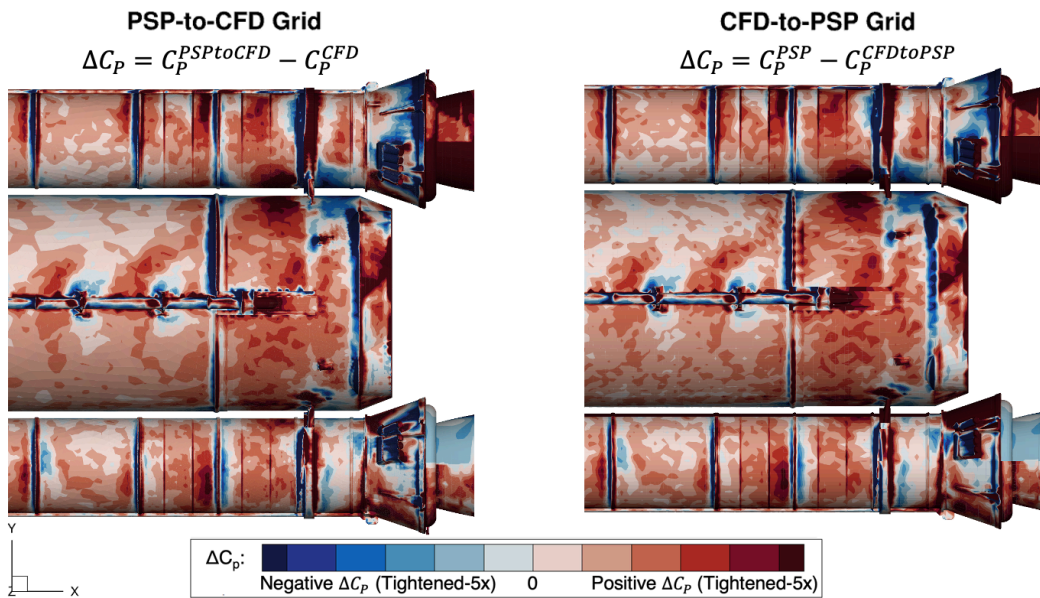
PSP-to-CFD Grid
$$\Delta C_P = C_P^{PSPtoCFD} - C_P^{CFD}$$

CFD-to-PSP Grid
$$\Delta C_P = C_P^{PSP} - C_P^{CFDtoPSP}$$

ΔC_p:
Negative ΔC_P (Tightened-5x)   0   Positive ΔC_P (Tightened-5x)

Fig. 12   Aft SRB region at M_∞ = 1.3, α_V = 0°, β_V = 8°, and Re_u = 3 x 10⁶/ft.

3. LAS/MPCV Region

Figures 13 and 14 show a side-by-side comparison between the LAS/MPCV region for both grids at $M_\infty = 1.3$, α_V = 0°, β_V = 8°, Re_u = 3 x 10^6/ft, and Re_D = 1.08 x 10^6. This area of the rocket exhibits the most clear view of how the different grid densities affects the ΔC_P contours generated by each interpolation method. The large protuberance on the right side of the figures, also known as the LAS umbilical, creates flow physics that are difficult to model, both in CFD and in the wind tunnel. On both grids, the area directly behind the protuberance has a high positive ΔC_P, meaning that the CFD or CFD-interpolated data register a much higher C_P around this area than the PSP or PSP-interpolated data. To further complicate things, this high-ΔC_P region feeds directly into the start of a ridge, where ΔC_P is typically negative, meaning that the CFD/CFD-interpolated data quickly switches from overpredicting C_P to underpredicting C_P when compared to the PSP/PSP-interpolated data. Figure 13, which uses the PSP-to-CFD grid, is able to capture this region and show a smooth transition between the two areas, while Fig. 14, which uses the CFD-to-PSP grid, has a break in continuity near the start of the ridge. While this doesn't mean that one grid is necessarily 'better' than the other grid, it is important to note the differences between the two methods, and to factor this behavior in when performing future analyses.
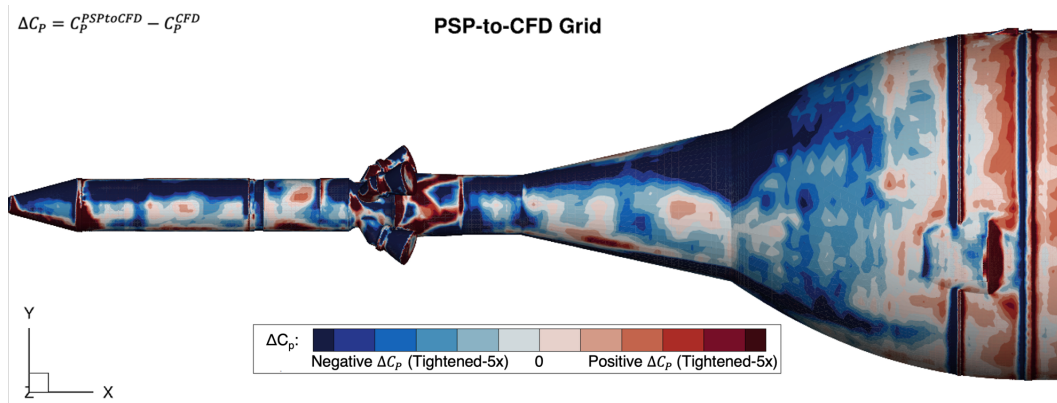

Fig. 13 **PSP data interpolated onto the CFD surface grid at M_∞ = 1.3, α_V = 0°, β_V = 8°, and Re_u= 3 x 10^6/ft.**
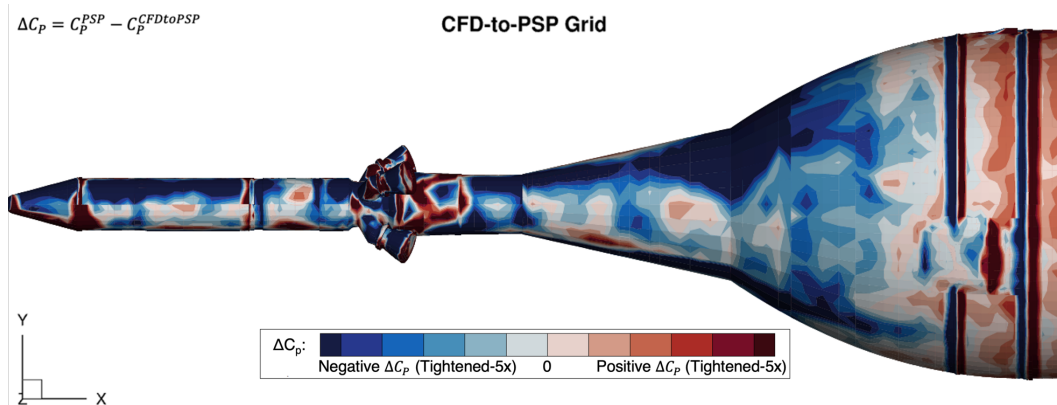

Fig. 14 **CFD data interpolated onto the PSP surface grid at M_∞ = 1.3, α_V = 0°, β_V = 8°, and Re_u = 3 x 10^6/ft.**

B. Lineloads

Lineloads were calculated with a different code base when the dataset was originally developed [4]. This new technique differs from the existing one in two ways: the treatment of blanked surface regions where PSP data does not exist, and the order of the integral approximation. Comparisons between the reference lineloads and those generated as part of this workflow are presented in this subsection.

Figures 15 and 16 present four lineloads each as computed on the SLS core stage and on one of the boosters. The

lineloads computed from the CFD pressure data are presented in black while those computed from the PSP data are presented in red. The reference lineloads are presented as dashed lines while the lineloads from this new method are presented as solid lines. The left column shows the axial force coefficient lineloads (CA_{LL}), the central column shows the side force coefficient lineloads (CY_{LL}), and the right column shows the normal force coefficient lineloads (CN_{LL}).
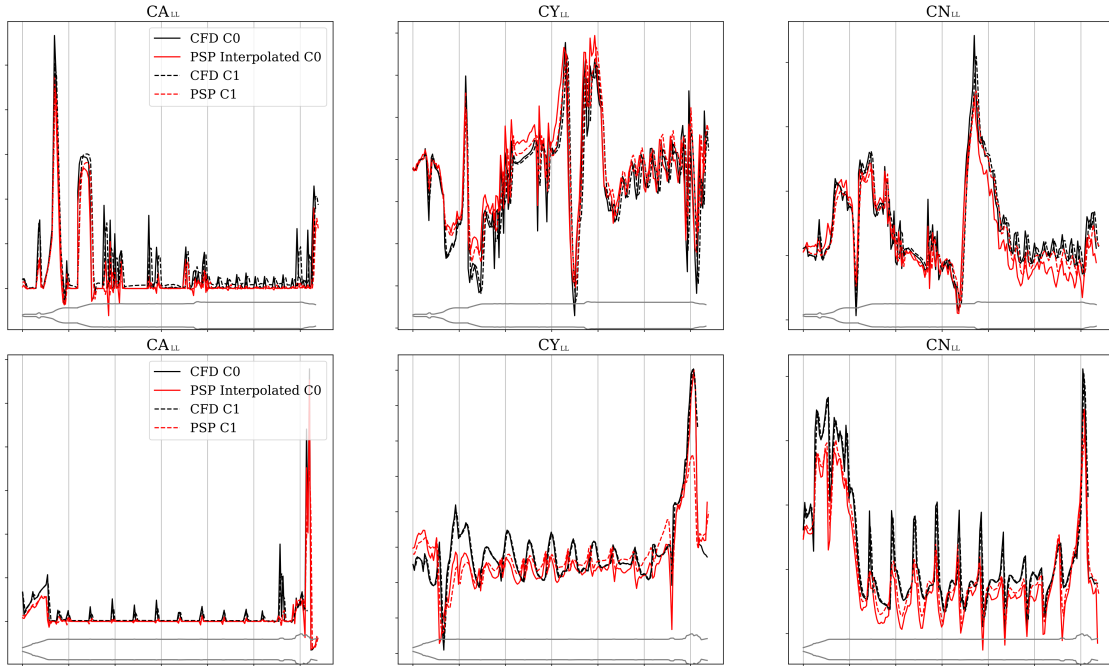

Fig. 15   Lineloads computed at a particular aerodynamic orientation with the new and the reference methods on both the CFD and the PSP data. 201 lineload bins were used in all cases.
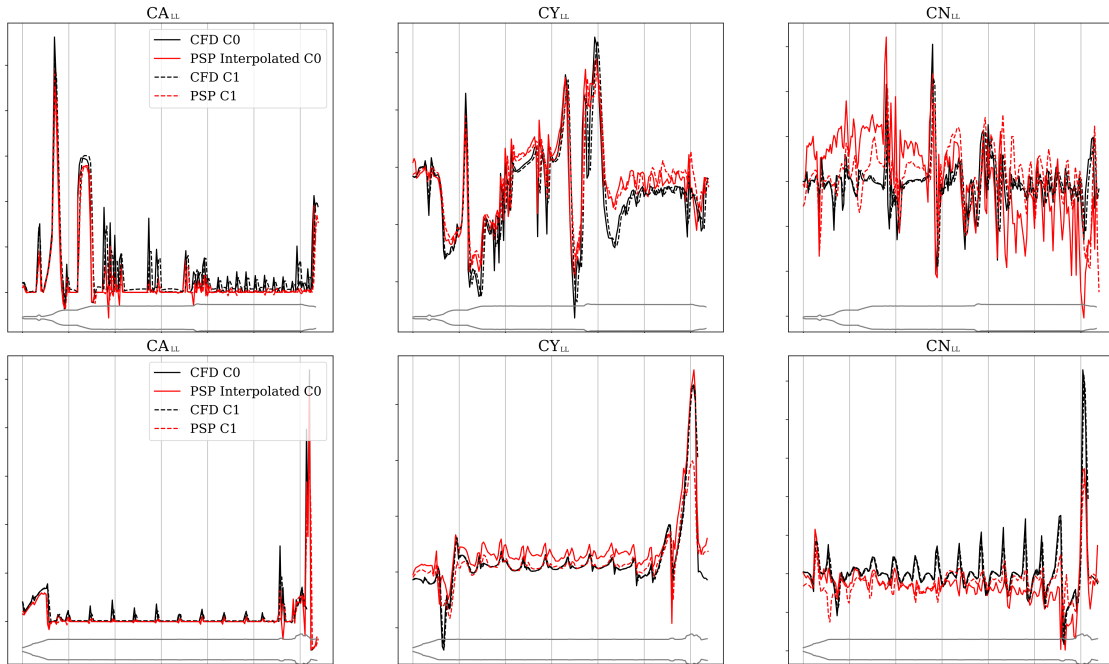

Fig. 16   Lineloads computed at a different aerodynamic orientation with the new and the reference methods on both the CFD and the PSP data. 201 lineload bins were used in all cases.

The negligible differences between the dashed and solid black lines – the two lineloads computed on the same CFD pressure data – quantifies the minor effect that the integration order has on the resulting lineloads. These lineloads are computed on identical surface data, but the dashed lines are created using C^1 integration akin to the trapezoid rule while the solid lines are created using C^0 integration akin to the midpoint rule. The CFD lineloads appear to be virtually identical save for a half-bin shift in x caused by the difference in bin definition. These lines are deemed identical for engineering use.

The difference in the PSP lineloads is, by comparison, more substantial. The main difference in the two approaches is highlighted especially in the CY booster lineloads in Fig. 16. The new method interpolates PSP data onto blanked regions shown in blue in Fig. 5, whereas the reference method leaves the blanked regions out of consideration entirely. Both approaches have their merits; including approximations of the blanked regions makes the PSP data more directly comparable to the CFD data whereas ignoring blanked regions prevents approximations from altering the trends established by the PSP data itself.

IV. Conclusion

This work introduced a method to use data mapping and grid interpolation to compare PSP data collected from wind tunnel experiments with CFD data extracted from post-test simulations for NASA's SLS. The data sets used to perform this work were pulled from a 2016 NASA Ames UPWT test, which tested three different configurations of the SLS over a period of several months. This work also introduced a method to compute lineloads using a different integration scheme, and comparisons of lineloads extracted from both the PSP and CFD-mapped data were made.

Overall, the PSP-to-CFD surface pressure variations compare favorably with the CFD-to-PSP surface pressure variations in most regions. Differences tend to occur around ridges or abrupt changes in curvature, and are likely present due to the differing resolutions between the CFD and PSP surface grids. Of the two, the CFD surface grid is of a higher resolution, has no blanked regions, and is easier to extract lineloads from than the PSP surface grid. The CFD surface grid is also able to capture changes in curvature more smoothly. Despite their differences, however, both surface grids still compare quite well and suggest that the quality of the data is not altered significantly as a result of using the new interpolation method.

Comparisons to lineloads generated from a previously conducted study and the new lineloads code were performed. Changing the integration from C^1 to C^0, or from the trapezoid to the midpoint rule, had little effect on the lineloads calculated from the CFD surface grid. Notable differences were observed on the PSP surface grid, however, and are present because the new method interpolates PSP data onto blanked regions, where the reference method chooses to ignore them entirely. Both approaches have their strengths, as the new method allows for more direct comparisons from PSP to CFD data to be made, while the reference method simply presents the data as it is and does not seek to interpolate into regions where it wasn't present to begin with.

PSP and CFD surface grids are often generated using different methods, but this work suggests mapping the data from one grid to another still provides a strong basis for data comparison. It may be useful to generate a singular common surface grid for both CFD and PSP data to circumvent this process, but the respective grids are often created with vastly different objectives and it may be difficult to resolve this. This method will continue to be developed over time, with the intention of applying it to tests where PSP and potentially uPSP are used in the future.

Acknowledgments

References

[1] "Space Launch System," Available at `https://www.nasa.gov/exploration/systems/sls/index.html`, 2021.

[2] McMillin, S. N., Shea, P. R., Dalle, D. J., Rogers, S. E., Roozeboom, N. H., Meeroff, J. G., and Lee, H. C., "Comparison of Space Launch System Aerodynamic Surface Pressure Measurements from Experimental Testing and CFD," *AIAA Aviation Forum*, 2019.

[3] Roozeboom, N. H., Powell, J., Baerny, J. K., Murakami, D. D., Ngo, C. L., Garbeff, T. J., Ross, J. C., and Flach, R., "Development of Unsteady Pressure-Sensitive Paint Application on NASA Space Launch System," *AIAA Aviation Forum*, 2019.

[4] Meeroff, J. G., Lee, H. C., Dalle, D. J., Rogers, S. E., Roozeboom, N. H., and Baerny, J. K., "Comparison of SLS Sectional Loads from Pressure Sensitive Paint and CFD," *AIAA SciTech Forum*, 2019.

[5] Holmberg, J., "NASA Ames Research Center Wind Tunnel Division, Test Planning Guide for High Speed Wind Tunnels," A027-9391-XB2, Revision 6.

[6] Kmak, F., "Modernization and Activation of the NASA Ames 11- by 11-Foot Transonic Wind Tunnel," *21st AIAA Aerodynamic Measurement Technology and Ground Testing Conference*, 2002.

[7] Kmak, F., "Capabilities of the Unitary Plan Wind Tunnel (Oral Presentation)," *55th AIAA Aerospace Sciences Mtg.*, 2017.

[8] Shea, P. R., Pinier, J. T., Houlden, P. R., Faveregh, A. L., Hemsch, M. J., Dalle, D. J., Rogers, S. E., Meeroff, J. G., and Lee, H. C., "Ascent Aerodynamic Force and Moment Database Development for the Space Launch System," *AIAA SciTech Forum*, 2019.

[9] Lee, M. W., and Wignall, T. J., "A Python Module for Surface Lineloads Integation," NASA TM-2021-XX, In preparation.

[10] Chan, W. M., Pandya, S. A., Rogers, S. E., Jensen, J. C., Lee, H. C., Kao, D. L., Buning, P. G., Meakin, R. L., Boger, D. A., and Nash, S. M., "Chimera Grid Tools User's Manual," Available at `https://www.nas.nasa.gov/publications/software/docs/chimera/pages/man.html`, 2018.

[11] Chan, W. M., "Overset grid technology development at NASA Ames Research Center," *Computers & Fluids*, Vol. 38, No. 3, 2009, pp. 496–503.